Enhancing Robotic Interaction: A Fractional-Order Impedance Control Strategy to Mitigate Overshooting and Improve Tracking in Dynamic Environments

Hongli Cao

Taiyuan city vocational college

Taiyuan, China

Email: chl_xueshu@126.com, ORCID: 0000-0003-4324-3785

***Abstract*—This research investigates the difficulties associated with transient overshooting, sluggish tracking responses, and inadequate steady-state accuracy that occur during the dynamic interactions between robotic systems and their physical environments. To tackle these challenges, a fractional-order impedance control strategy for robotic systems is proposed. An initial evaluation of existing integer-order impedance control methods indicates that these approaches depend on modifications to the update rate and adjustments to the elasticity parameter to suit various tasks. In light of these constraints, this study presents a more adaptable fractional-order impedance control framework. By utilizing the intrinsic characteristics of fractional-order impedance, the gain coefficients are designed to enable the mapping of fractional-order impedance to integer-order impedance, thereby improving computational efficiency and practical applicability. Additionally, certain beneficial aspects of high integer-order impedance control are incorporated into the fractional-order impedance to enhance overall performance, with clearly defined boundaries for dynamic adjustments. Simulation results indicate that the proposed fractional-order impedance significantly diminishes the peak contact force overshoot during contact and effectively reduces the system's unstable oscillatory behaviours. This approach is particularly advantageous for applications in which robots must function and interact within dynamic and uncertain environments.**

***Keywords*— force control, fractional order, contact process, overshoot, impedance**

1. Introduction

The swift progression of robotics technology has resulted in the reduction of conventional operational limitations, facilitating the incorporation of robotic systems into diverse human environments and external physical contexts. This integration is particularly prominent in domains such as human-robot collaboration in precision assembly, robot-assisted precision machining, and medical rehabilitation employing robotic arms [1,2]. As a result, the challenge of effectively managing the dynamic contact processes between robots and their physical environments has gained increasing importance. The contact force generated during these dynamic interactions frequently approaches a critical threshold; surpassing this limit can lead to excessive contact forces at the moment of interaction, which may result in task failure and significant production accidents. Such contact overshoot can stem from various factors, including delays in measurement feedback, communication lags, inaccuracies in robot modeling, environmental dynamics, and discontinuities in control inputs. To tackle this intricate issue, researchers both domestically and internationally have proposed a range of adaptive control methodologies.

The predominant methodologies for regulating compliance in robotics encompass hybrid position-force control and impedance control. The hybrid position-force control framework, originally proposed by Raibert, distinguishes the robot's degrees of freedom from its geometric tasks, thereby partitioning the task space into two distinct subspaces: one focused on position and the other on force. Within this framework, position tracking control is executed in the unconstrained position space, while force feedback control is applied in the force-constrained space. Hogan further advanced this concept by elucidating the interaction between motion and force, coining the term impedance control to describe this relationship. Generally, impedance control demonstrates superior robustness compared to hybrid

position-force control in most dynamic contact scenarios encountered in robotics. However, the intuitive and straightforward nature of hybrid position-force control frequently leads to its integration with impedance control to tackle more intricate dynamic contact challenges. Noteworthy applications of this integrated approach include the seamless transition from unconstrained to constrained spaces during robotic arm assembly in unpredictable environments, the rehabilitation of patients utilizing upper extremity exoskeletons, and the regulation of human force in robotic sanding operations.

In order to overcome the constraints inherent in numerous industrial robots, which primarily operate in position control modes and lack the ability to directly execute impedance control, various researchers have established a position-based impedance control framework [8-12]. Duan [9] successfully regulated the contact force of a robotic arm by deriving the desired position trajectory from the force deviations encountered during the grinding process. To address the issue of adjusting the dynamic update rate in position-based impedance control, Cao introduced a practical and straightforward adjustment method [11]. Furthermore, Sheng [12] addressed the potential risk of component damage resulting from contact force overshoot during the machining of large thin-walled parts by robots, proposing an impedance control strategy that employs fuzzy control to modulate the dynamic update rate.

In recent years, a significant number of researchers have focused their investigations on a particular domain of nonlinear control known as fractional-order impedance control. This approach has demonstrated superior stabilization capabilities when compared to conventional integer-order impedance control [13]. The unique memory characteristics of fractional-order impedance positively influence both transient response and steady-state tracking, thereby enhancing the performance of closed-loop systems [14]. This enhancement is especially evident in applications aimed at improving the stability of human-machine physical interactions [15] and the adaptability of exoskeleton wearable robots [16]. Nevertheless, the computation of fractional-order impedance presents substantial challenges. The difficulties associated with real-time computation and practical implementation remain considerable barriers. Oustaloup has proposed a methodology that utilizes frequency response fitting to derive an approximate integer-order transfer function from the fractional-order model [17], a technique that has gained significant popularity in contemporary applications. Despite these advancements, the computational demands remain complex, necessitating a careful equilibrium between practicality and sophistication. Furthermore, there is a notable deficiency in the literature concerning the modeling and performance distinctions between fractional-order and integer-order impedance. Additionally, the impact of fractional-order impedance during dynamic contact interactions between robots and their environments, along with the corresponding implementation strategies, warrants further academic investigation.

This research investigates the challenges associated with contact overshoot, response speed, and tracking accuracy that arise during the dynamic interactions between robotic systems and their environments. To enhance stability during the contact phase, we propose an improvement in contact behavior through the application of fractional-order impedance design. Our analysis begins with a review of the characteristics of existing integer-order impedance control in the context of the contact process, which serves as a foundation for the development of fractional-order impedance control. By leveraging the inherent properties of fractional-order impedance, we derive percentage gain coefficients that facilitate the mapping of fractional-order impedance to integer-order impedance, thereby optimizing computational efficiency and practical implementation. Additionally, we incorporate specific attributes of integer-order impedance into the fractional-order impedance framework to further enhance performance. Ultimately, we conduct simulations to evaluate and compare the contact performance of various robotic systems operating in dynamic environments, thereby demonstrating the effectiveness of the proposed fractional-order impedance control approach.

2. Preliminary

2.1. Fractional order calculates

The fractional-order (FO) calculus, which extends the conventional integer-order (IO) calculus, enables the differentiation and integration of arbitrary orders. The computation of an FO derivative or integral presents a complex challenge, as there are several mathematically rigorous definitions available, each contingent upon the specific application in question. Notably, the Grunwald-Letnikov definition is frequently utilized for the calculation of fractional-order operations. The formal expression for the Grunwald-Letnikov definition in the context of FO operations is as follows:

$$D^{\alpha}y(t) = \lim_{h\to 0} \frac{1}{h^{\alpha}} \sum_{i=0}^{\frac{t-a}{h}} C_i^{\alpha}\, y(t-ih) \tag{1}$$

α is the order, h is the step size of the calculation, a is the window length, and C_i^{α} can be calculated by following:

$$C_0^{\alpha} = 1,\ C_i^{\alpha} = C_{i-1}^{\alpha}\left(1 - \frac{\alpha+1}{i}\right),\ i = 1,2,\dots \tag{2}$$

The differential integral functions as a linear operator characterized by both a memory component and a forgetting factor that is contingent upon the entire trajectory of the data. In real-time applications, it predominantly adheres to the principles of short-term memory, influenced by the forgetting factor. Consequently, this reliance on memory and computational resources can lead to significant challenges in practical implementations.

2.2. Classical Impedance Control

Position-based impedance control represents a methodological framework that integrates the monitoring of a robot's positional parameters with an impedance control strategy. This approach involves the collection of contact data, the calculation of positional deviations, and the adjustment of the desired trajectory through impedance control techniques. Additionally, it allows for motion tracking within the robot's specified operational space, thereby promoting compliant interactions during contact, as illustrated in Figure 1.

The impedance function is frequently selected as a linear second-order model of the following form,

$$G(s) = \frac{1}{m_d s^2 + b_d s + k_d} \tag{3}$$

Here, m_d and b_d are the desired parameters of impedance controller. The linear second-order model exhibits a discrepancy in the tracking of contact force under steady-state conditions [9].

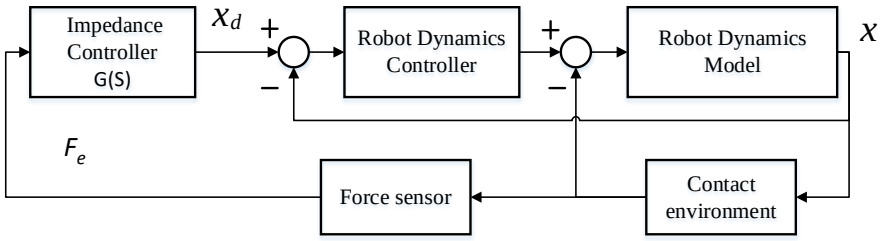

Figure 1 Simplified model of robot-environment interaction

$$e_{fss} = \lim_{s \to 0} s e_f(s) = \frac{k_d}{k_d + k_e}(k_e(x - x_d) - f_d) \tag{4}$$

Equation (4) illustrates that the effective reduction of the steady-state tracking error through impedance control requires accurate feedback concerning both the position and stiffness of the measurement environment in order to appropriately adjust the impedance parameters. Nonetheless, this undertaking poses considerable practical difficulties. An alternative approach involves eliminating the elastic component from the impedance model and incorporating compensation for the dynamic environment, which facilitates the advancement of adaptive impedance control, as discussed in the subsequent sections,

$$G(s) = \frac{1}{m_d s^2 + b_d(s + \rho(s))} \tag{5}$$

Adaptive impedance control is linked to the occurrence of overshooting, a phenomenon that results from the exclusion of the elasticity term. This exclusion impedes the gradual dissipation of energy that typically transpires during the contact phase between the robotic system and its surrounding environment. Furthermore, the compensation term utilized in adaptive impedance control functions at an elevated update rate, which improves steady-state tracking accuracy; however, it simultaneously leads to oscillatory overshooting behavior during contact [10]. Therefore, it is essential to implement dynamic adjustments to the update rate. To mitigate this challenge, a dynamic adaptive impedance control strategy is proposed, which takes into account both transient and steady-state behaviors [11, 12].

The traditional methodology for implementing impedance control in dynamic interactions between a robot and its environment can be articulated as follows: In the initial phase of a collision or contact event, it is recommended to either augment the elastic component of the impedance or reduce the update frequency to alleviate overshooting and instability. Conversely, during the steady-state tracking or operational phase, the elastic component may be removed or the update frequency increased to improve tracking accuracy.

3. Fractional order-based impedance control

3.1 Adaptive fractional-order impedance control

Drawing from the fundamental concepts of integer-order adaptive impedance control design [18-20], the parameter associated with second-order differentiation in fractional-order impedance has been adjusted from an integer to a fractional value,

$$Y(s) = \frac{1}{Z_{FO-AIC}(s)} = \frac{1}{m_d s^{\alpha} + b_d(s + \rho(s))} \tag{6}$$

$$\rho(s) = -\frac{\sigma}{b} e_f(s) \tag{7}$$

Equation (7) defines the adaptive compensation law, ρ is the damping compensation which adjusted according to the force sensor information online. Consequently, fractional order impedance incorporates a greater number of order parameters in comparison to integer order impedance α ($1 < \alpha < 2$). The proposed methodology facilitates the alteration of the dynamic interaction characteristics between the robot and its environment, thereby enhancing the adaptability of control strategy development. When the system operates at lower extremes, it employs first-order damped control. Conversely, at higher extremes, it transitions to second-order integer-order impedance control. A notable feature of this system is that as the order decreases, the ability to store inertial energy gradually declines,

leading to an increased focus on energy dissipation. This transformation can be expressed in the frequency domain as follows,

$$Z = m_d\omega^{\alpha}\, cos\left(\frac{\alpha\pi}{2}\right) + b_d(j\omega + \rho(j\omega)) + jm_d\omega^{\alpha}\, sin\left(\frac{\alpha\pi}{2}\right) \tag{8}$$

From equation (8), it can be observed that the effective mass and effective damping of the fractional order impedance are, $m_d\omega^{\alpha}\, sin(\alpha\pi/2)$ and $m_d\omega^{\alpha}\, cos(\alpha\pi/2) + b_d\big(j\omega + \rho(j\omega)\big)$, respectively. The general integer order impedance is characterized by fixed constants. As a result, the effective damping and mass properties of fractional order systems exhibit behavior that is dependent on frequency, a factor that is particularly significant in the management of dynamic contact processes. Lowering the order of the fractional order impedance can markedly enhance the stability and robustness of a robot's interactions with its surrounding environment, as can be seen in Figure 2.

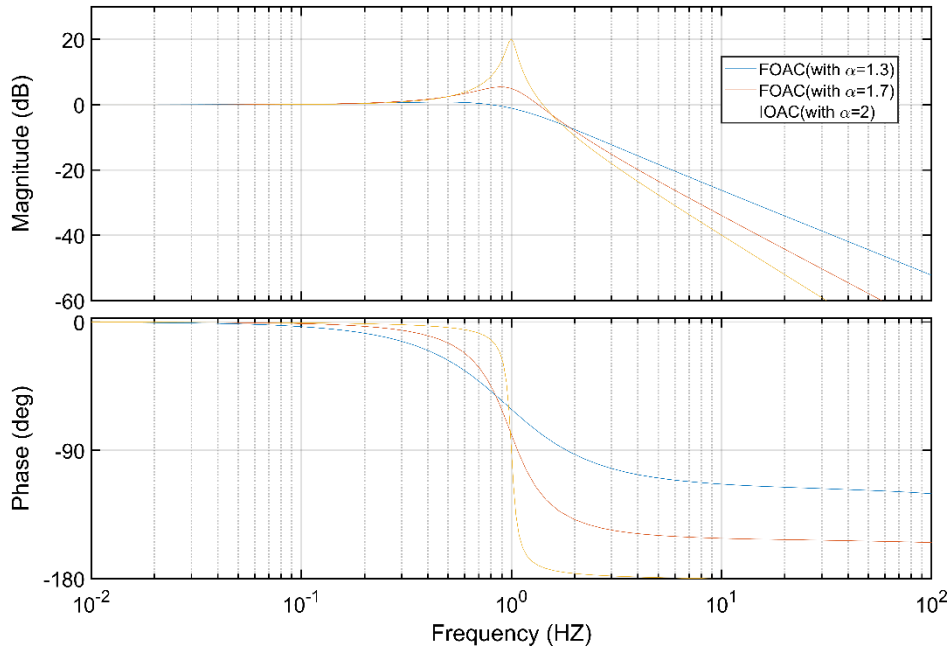

FIGURE 2 Bode diagram analysis of FO-AIC and IO-AIC

3.2 Fractional-order impedance approximations

Indirect approximation algorithms that are commonly utilized encompass continuous fractional methods, along with the techniques formulated by Chareff and Oustaloup, among others. It is essential to note that although Oustaloup exhibits proficient approximation abilities, its applicability is restricted to particular scenarios. Additionally, the computational requirements associated with fractional order calculus are significantly intricate.

The intrinsic natural characteristics of fractional order impedance indicate that the effective mass and damping are influenced by the order of the system. Consequently, this paper employs a percentage factor $\beta = \alpha - 1$ $(0 < \beta < 1)$ associated with two integer order controllers, utilizing a specified limit value to achieve the approximation. This approximation is modulated by the duty cycle, as outlined below,

$$Y(s) = \frac{\beta}{m_d s^2 + b_d\big(s + \rho(s)\big)} + \frac{(1-\beta)}{b_d\big(s + \rho(s)\big)} \tag{9}$$

According to equation (9), the coefficients are instrumental in determining the effective mass and damping in accordance with the fractional order impedance approximation, suggesting that the order has a comparable regulatory influence.

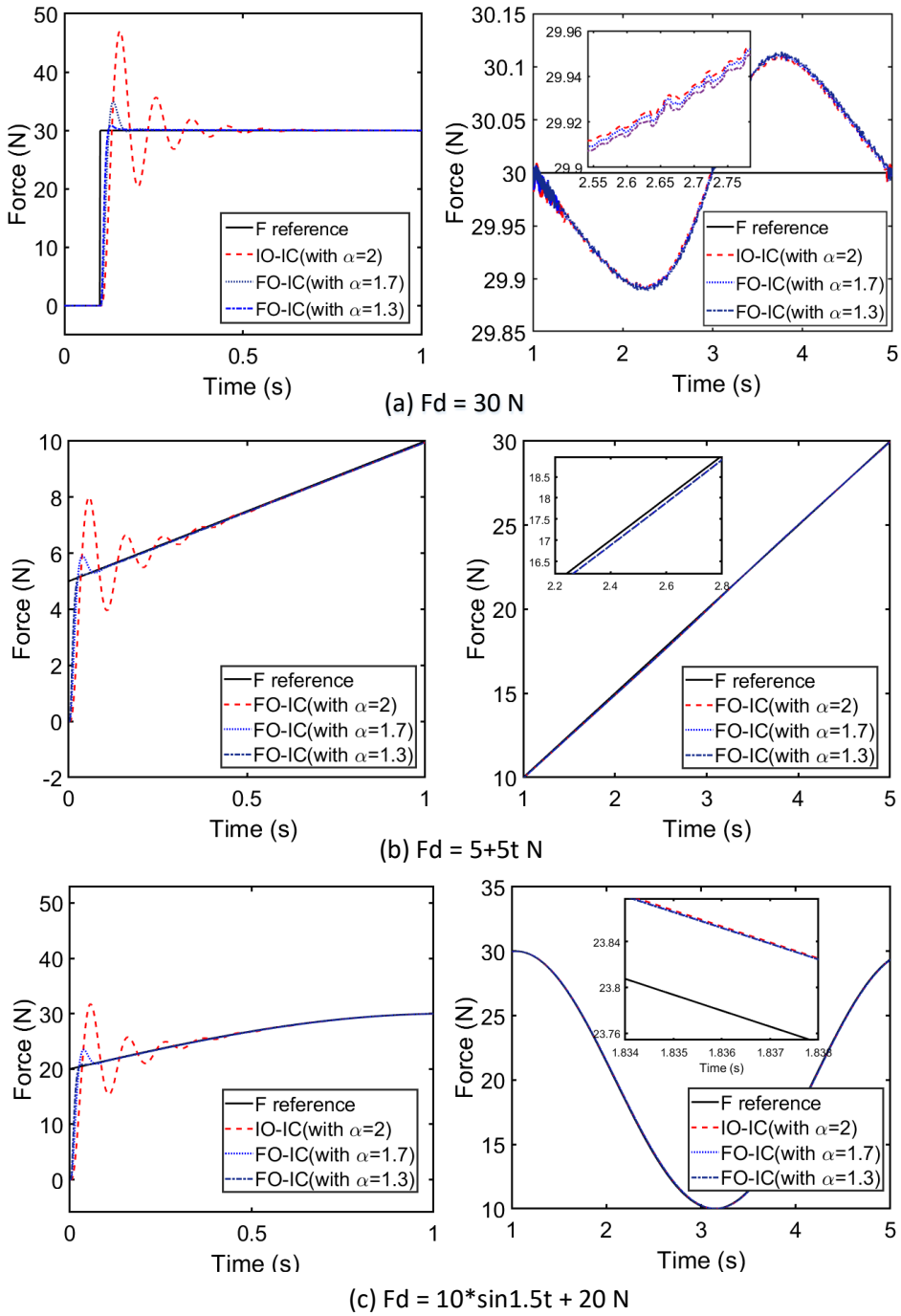

FIGURE 3 Performance comparison of FO-AIC and IO-AIC for (a) constant force; (b) slope force; (c) sine force with dynamic stiffness.

Figure 3 presents the simulation outcomes for the fractional order active impedance control (FO-AIC) and the integer order active impedance control (IO-AIC) under three different force conditions: a constant force, a slope force, and a sine force. The time intervals from 0 to 1 second represent the initial contact phase, while the period from 1 to 5 seconds corresponds to the tracking phase. Observations during the contact phase reveal that as the order decreases, the magnitude of force overshoots also diminishes, indicating that a lower order results in reduced collision forces.

Furthermore, while there is a slight enhancement in force tracking during the tracking phase, the improvement is not substantial. Consequently, the proposed FO-IC demonstrates a significant reduction in force overshoots during the initial contact phase when compared to the IO-IC, exhibiting considerable adaptability and robustness across various tasks.

3.3 Adaptive boundaries

The stability and response time of fractional-order impedance control are affected by factors beyond merely the approximation coefficients and the compensation rate. The comprehensive representation of adaptive fractional-order impedance in the time domain is delineated as follows,

$$e_f(t) = \frac{m_d}{\beta}\ddot{e}(t) + \frac{b_d}{\beta(1-\beta)}\left(\dot{e}(t) + \rho(t)\right) \tag{10}$$

$$\rho(t) = \sigma\beta(1-\beta)\frac{\left(f_d(t-T) - f_e(t-T)\right)}{b_d} + \rho(t-T) \tag{11}$$

Where the environmental reference position is estimated to be $\hat{e} = e + \delta p_e$. The initial moment $\rho(0) = 0$, is the sampling period. T is the sampling period. σ is the update rate, and the following analysis determines the dynamic adjustable range.

By combining the $\hat{e}(t) = e(t) + \delta p_e(t)$ into equation (10) as follows:

$$\frac{m_d}{\beta}\ddot{e}(t) + \frac{b_d}{\beta(1-\beta)}\dot{e}(t) - e_f(t) + \frac{b_d}{\beta(1-\beta)}\rho(t-T) + \sigma\left(f_d(t-T) - f_e(t-T)\right)$$
$$= -\frac{m_d}{\beta}\delta\ddot{p}_e(t) - \frac{b_d}{\beta(1-\beta)}\delta\dot{p}_e(t) \tag{12}$$

Setting up the elastic contact environment $f_e = -k_e e$ and bring its differential form into (12) can be obtained:

$$-\frac{m_d}{\beta}\ddot{f}_e(t) - \frac{b_d}{\beta(1-\beta)}\dot{f}_e(t) - k_e e_f(t) + \frac{b_d}{\beta(1-\beta)}k_e\rho(t-T) + \sigma k_e(f_d(t-T) - f_e(t-T)$$
$$= -k_e\left(\frac{m_d}{\beta}\delta\ddot{p}_e(t) + \frac{b_d}{\beta(1-\beta)}\delta\dot{p}_e(t)\right) \tag{13}$$

Let the contact force estimation error$\hat{f}_e(t) = k_e\delta p_e(t)$, and add a fixed constant term to both sides of equation (13),the term $\frac{m_d}{\beta}\ddot{f}_d(t) + \frac{b_d}{\beta(1-\beta)}\dot{f}_d(t)$ that can be obtained:

$$\frac{m_d}{\beta}\left(\ddot{f}_d(t) - \ddot{\hat{f}}_e(t)\right) + \frac{b_d}{\beta(1-\beta)}\left(\dot{f}_d(t) - \dot{\hat{f}}_e\right) - k_e e_f(t) + \frac{b_d}{\beta(1-\beta)}k_e\rho(t-T) + \sigma k_e\left(f_d(t-T) - f_e(t-T)\right)$$
$$= \frac{m_d}{\beta}\left(\ddot{f}_d(t) - \ddot{\hat{f}}_e(t)\right) + \frac{b_d}{\beta(1-\beta)}\left(\dot{f}_d(t) - \dot{\hat{f}}_e(t)\right) \tag{14}$$

Mark $c(t) = f_d(t) - f_e(t)$ and$r(t) = f_d(t) - \hat{f}_e(t)$, the compensation term is expanded and incorporated into equation (14),

$$\frac{m_d}{\beta}\ddot{c} + \frac{b_d}{\beta(1-\beta)}\dot{c} + k_e c + \sigma k_e\left(c(t-(n+1)T) + \cdots + c(t-T)\right) = \frac{m_d}{\beta}\ddot{r} + \frac{b_d}{\beta(1-\beta)}\dot{r} \tag{15}$$

The Laplace transformation of Equation (15) produces,

$$\frac{c(s)}{r(s)} = \frac{(1-\beta)m_d s^2 + b_d s}{\begin{array}{l}(1-\beta)m_d s^2 + b_d s + k_e\beta(1-\beta) \\ +\sigma k_e\beta(1-\beta)(e^{-(n+1)Ts} + \cdots + e^{-Ts})\end{array}} \tag{16}$$

Approximating the superposition term $\sum_{n=1}^{\infty} e^{-nTs} \cong (1-Ts)/Ts$ approximation and bring it into the characteristic equation can be obtained:

$$(1-\beta)m_d T s^3 + b_d T s^2 + k_e T(\beta(1-\beta)-\sigma)s + \sigma k_e = 0 \tag{17}$$

According to The Rouse Stability Criterion, equation (17) can be computed as follows,

$$\begin{array}{lll} s^3 & (1-\beta)m_d T & k_e T(\beta(1-\beta)-\sigma) \\ s^2 & b_d T & \sigma k_e \\ s^1 & \dfrac{b_d T^2 k_e(\beta(1-\beta)-\sigma) - (1-\beta)m_d T\sigma k_e}{b_d T} & 0 \\ s^0 & \sigma k_e & 0 \end{array} \tag{18}$$

To ensure the stability of the system, it is crucial that the coefficients retain positive values. The limitations regarding the update rate are established in the following manner,

$$\begin{cases} \dfrac{b_d T^2(\beta(1-\beta)-\sigma) - (1-\beta)m_d T\sigma k_e}{b_d T} > 0 \\ k_e T(\beta(1-\beta)-\sigma) > 0 \\ \sigma k_e > 0 \end{cases} \tag{19}$$

$$0 < \sigma < \frac{b_d T\beta(1-\beta)}{(1-\beta)m_d + b_d T} \tag{20}$$

3.4 Fuzzy logic controller

Supposing$[-X_{ef}, X_{ef}]$, $[-X_{\dot{e}f}, X_{\dot{e}f}]$and $[-Y_\sigma, Y_\sigma]$are the basic domains of e_f, $\dot{e}_f$ and σ respectively, in this study, A threshold of 10 has been established for simplification purposes. Following an analysis of the impact of various membership function types on the performance of fuzzy controllers, a total of seven triangular membership functions have been selected to represent the inputs and outputs of the proposed controller, as depicted in Figure 4. These functions correspond to seven linguistic values: positive big (PB), positive medium (PM), positive small (PS), zero (ZO), negative big (NB), negative medium (NM), and negative small (NS). The choice of triangular membership functions is primarily motivated by considerations of computational efficiency. Furthermore, the same membership functions have been employed for both input and output to facilitate calculations.

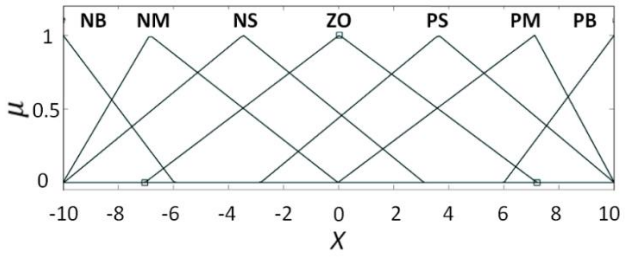

FIGURE 4 Membership function of e_f, $\dot{e}_f$ and σ.

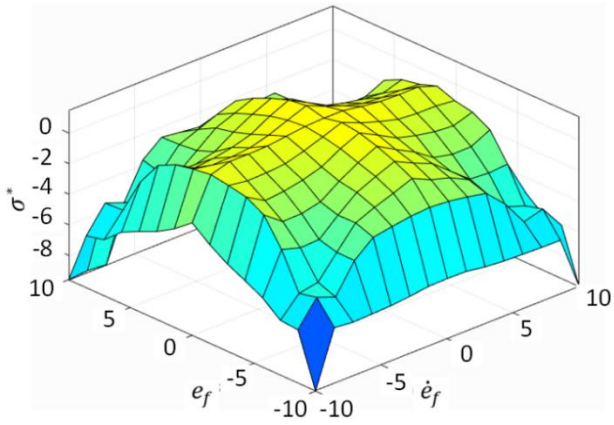

FIGURE 5 Output curve-surface of fuzzy logic control

Fuzzy control rules serve to generalize the relationships between inputs and outputs, and are formulated based on the experiences and intuitions of proficient practitioners in the field. Both the error e_f and the error ratio $\dot{e}_f$ have seven fuzzy subsets. Therefore, 49 fuzzy rules can be obtained according to the expertise, which are shown as TABLE 1.

The TABLE 1 can be applied as: if $e_f(i) = A_j$ and $\dot{e_f}(i) = B_j$, then $\sigma = C_j(j = 1, \dots, 49)$, A_j and B_j are the fuzzy sets corresponding to $e_f(i)$ and $\dot{e_f}(i)$ in the j-th fuzzy rule, respectively. C_j is the fuzzy outputs corresponding to σ in the j-th fuzzy logical rule. The membership grades for various fuzzy sets are obtained from the rule table through the application of the Mamdani fuzzy reasoning approach, as illustrated in Figure 5. The center of gravity defuzzification technique has been chosen to convert the output fuzzy set into a crisp value,

$$\sigma^* = \frac{\sum_{j=1}^{n} A_j(e_f)B_j(\dot{e_f})\mu_i}{\sum_{j=1}^{n} A_j(e_f)B_j(\dot{e_f})} \tag{21}$$

TABLE 1 Fuzzy Control Logic Rule Table

		$\dot{e}_f$						
		NB	**NM**	**NS**	**ZO**	**PS**	**PM**	**PB**
e_f	**NB**	NB	NB	NM	PM	NM	NB	NB
	NM	NB	NB	NM	PM	NM	NB	NB
	NS	NM	NM	NS	PS	NS	NM	NM
	ZO	NM	ZO	PM	PB	PM	ZO	NM
	PS	NM	NM	NS	PS	NS	NM	NM
	PM	NB	NB	NM	PM	NM	NB	NB
	PB	NB	NB	NM	PM	NM	NB	NB

Where n is the fuzzy rule number, μ_j is the membership grade of the j-th fuzzy output, which takes values in [0, 1]. Suppose Q_σ is the quantification factors of σ converting from the fuzzy domain to basic domain, which Q_σ can be given by:

$$Q_\sigma = \frac{B_\sigma}{10} \tag{22}$$

Then, the precise values of σ can be denoted as:

$$\sigma = Q_\sigma \sigma^* \tag{23}$$

In contemporary position-based impedance control systems, a hierarchical separation between position control

and impedance control has become a prevalent framework. This structure allows for the stability of the overall system to be analyzed as two distinct subsystems: impedance control and position control. It is a reasonable presumption that the position controller can maintain stable tracking in industrial robotic applications. Consequently, our primary focus is on the stability of the impedance control component. The stability of this component is primarily comprised of three elements: the pre-PID regulator, the fuzzy controller, and the fractional-order adaptive integral controller (FO-AIC). The pre-PID regulator enhances response speed and ensures tracking accuracy; however, it may also introduce significant overshoot. Conversely, fractional-order tools can effectively mitigate overshoot in force control, yet they fall short in terms of response time and tracking precision. The integration of fuzzy logic is essential for dynamic adjustment based on contact information, which can significantly influence both overshoot and tracking accuracy. Therefore, to achieve a force controller characterized by rapid response, minimal overshoot, and high tracking accuracy, the incorporation of all three components is crucial.

4. Simulation Experiment

This section outlines the design of two simulation experiments aimed at assessing the efficacy of the fractional-order impedance proposed in this study for enhancing and regulating the dynamic contact process within a robotic system.

4.1 1-DOF robot contact simulation

The single-degree-of-freedom robot is in contact with the environment as shown in Figure 6, assuming that the controlled single-degree-of-freedom robot has mass $m = 0.8$ kg , in order to estimate the mass $\hat{m} = 1$ kg. Design the basic impedance parameters $m_d = 1\ (\mathrm{N \cdot s^2})/\mathrm{m}$ and $b_d = 44\ \mathrm{Ns/m}$, and use this as a performance comparison benchmark for each impedance control strategy. The fractional order impedance approximation coefficients $\beta = 0.3$. Set the dynamic update rate in a variable range, i.e., from $0 \le \sigma \le 0.05$. Set$c_v = 1\ \mathrm{Ns/m}$, the $F_c = 3$ N be the coefficient of viscous friction and Coulomb friction, respectively, and the friction term denoted as $F_f = -sign(\dot{x})(c_v|\dot{x}| + F_c)$.

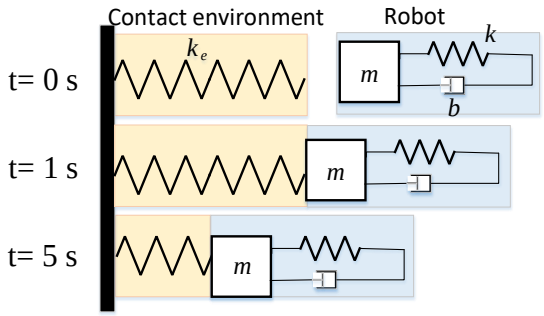

Figure 6 1-DOF robot contact process

A fixed-step solver is used for the simulation calculation, setting the sampling period $T = 4$ ms and input the desired force in the form of a step function with the value of $F_d = 30$ N. The stiffness environment is set to $k_e = 8000 + 800 \sin(\pi/2\ t)$.

Figure 7 illustrates a variety of traditional flexural control strategies employed during the contact phase, utilizing a standardized reference for impedance parameters. The strategies include Integral Order Impedance Control (IO-IC) [8], Adaptive Integral Order Impedance Control (IO-AIC) [9], Fuzzy Integral Order Adaptive Impedance Control (Fuzzy-IO-AIC) [12], as well as Fractional Order Impedance Control (FO-IC) and its derivatives, namely Fractional Order Adaptive Impedance Control (FO-AIC) and Fuzzy Fractional Order Adaptive Impedance Control (Fuzzy-FO-

AIC), which are introduced in this study. The IO-AIC demonstrates significant vibration and overshoot characteristics during the contact phase, with an overshoot magnitude of approximately 30 N. The hierarchy of overshoot magnitudes, ranked from highest to lowest, is as follows: Fuzzy-IO-AIC (15 N), IO-IC (15 N), FO-AIC (10 N), Fuzzy-FO-AIC (2 N), and FO-IC (2 N). This ranking indicates that both FO-IC and Fuzzy-FO-AIC exhibit superior capabilities in overshoot suppression. A comparative analysis of the cross-sectional results reveals that fractional-order impedance is more effective in reducing overshoot compared to its integer-order counterparts, a phenomenon attributed to its inherent damping characteristics. Furthermore, longitudinal comparisons indicate that lower update rates correlate with reduced overshoot magnitudes. Collectively, Fuzzy-FO-AIC and FO-IC demonstrate a dual damping effect, characterized by suppression linked to the intrinsic properties of fractional-order systems and the influence of decreased update rates. The steady-state tracking results during contact are depicted in Figure 8. The integer-order impedance controllers (IO-IC and FO-IC) exhibit suboptimal tracking performance, as evidenced by a tracking error ranging from 0.2 to 0.3 N. In contrast, the IO-AIC, FO-AIC, Fuzzy-IO-AIC, and Fuzzy-FO-AIC demonstrate enhanced tracking capabilities, with a tracking error of approximately 0.04 N. This finding suggests that the accuracy of steady-state contact force tracking is primarily influenced by the upper boundary value of the update rate, irrespective of the type of impedance controller (fractional-order or integer-order) employed. Additionally, it can be inferred that an increase in the update rate is associated with improved tracking accuracy.

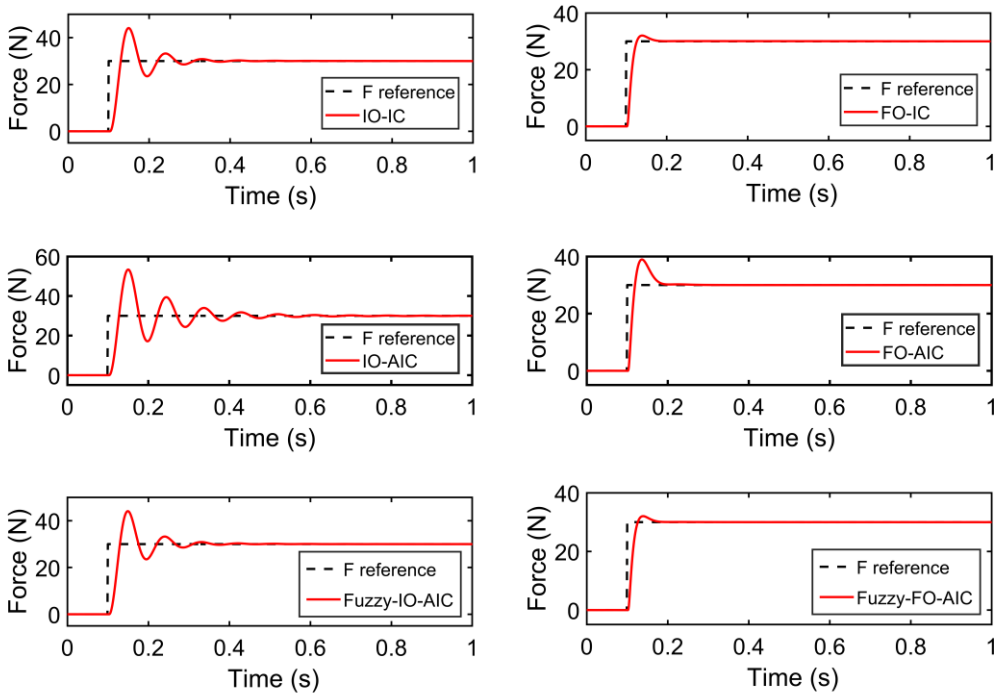

Figure 7 Transient response results at contact

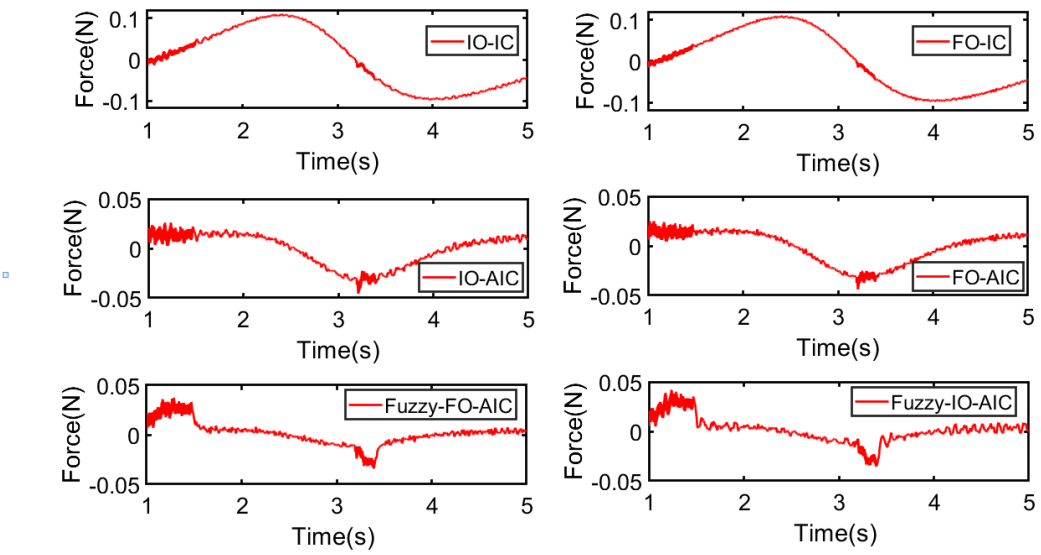

Figure 8 Steady-state tracking results at contact

To further assess the efficacy of fractional-order impedance in mitigating vibrational behavior, a comparative analysis was conducted on the dynamic contact performance of integer-order impedance controllers (IO-IC, Fuzzy-IO-AIC) relative to fractional-order impedance controllers (FO-IC, Fuzzy-FO-AIC) within a high-stiffness environment characterized by abrupt changes, as shown in Figure 9. At t = 4 seconds, a sudden increase in environmental stiffness resulted in significant contact overshooting for both integer-order and fractional-order impedance controllers. However, the fractional-order impedance controller exhibited a more rapid convergence to a steady state compared to its integer-order counterpart, indicating a more effective reduction of oscillatory behavior at this point.

During the interval from t = 6 to 8 seconds, an increase in environmental stiffness heightened the susceptibility of position-based impedance control to unstable contact behavior under high-stiffness conditions. This instability was particularly pronounced in the Fuzzy-IO-AIC, while the IO-IC exhibited only minor fluctuations that did not entirely dissipate. These findings suggest that a reduction in the update rate may provide some degree of suppression of such unstable behavior, although its effectiveness is limited. In contrast, the fractional-order impedance controller demonstrated a superior capacity to mitigate unstable vibrational behavior, thereby underscoring its stability and robustness—attributes that were less pronounced in the other controllers.

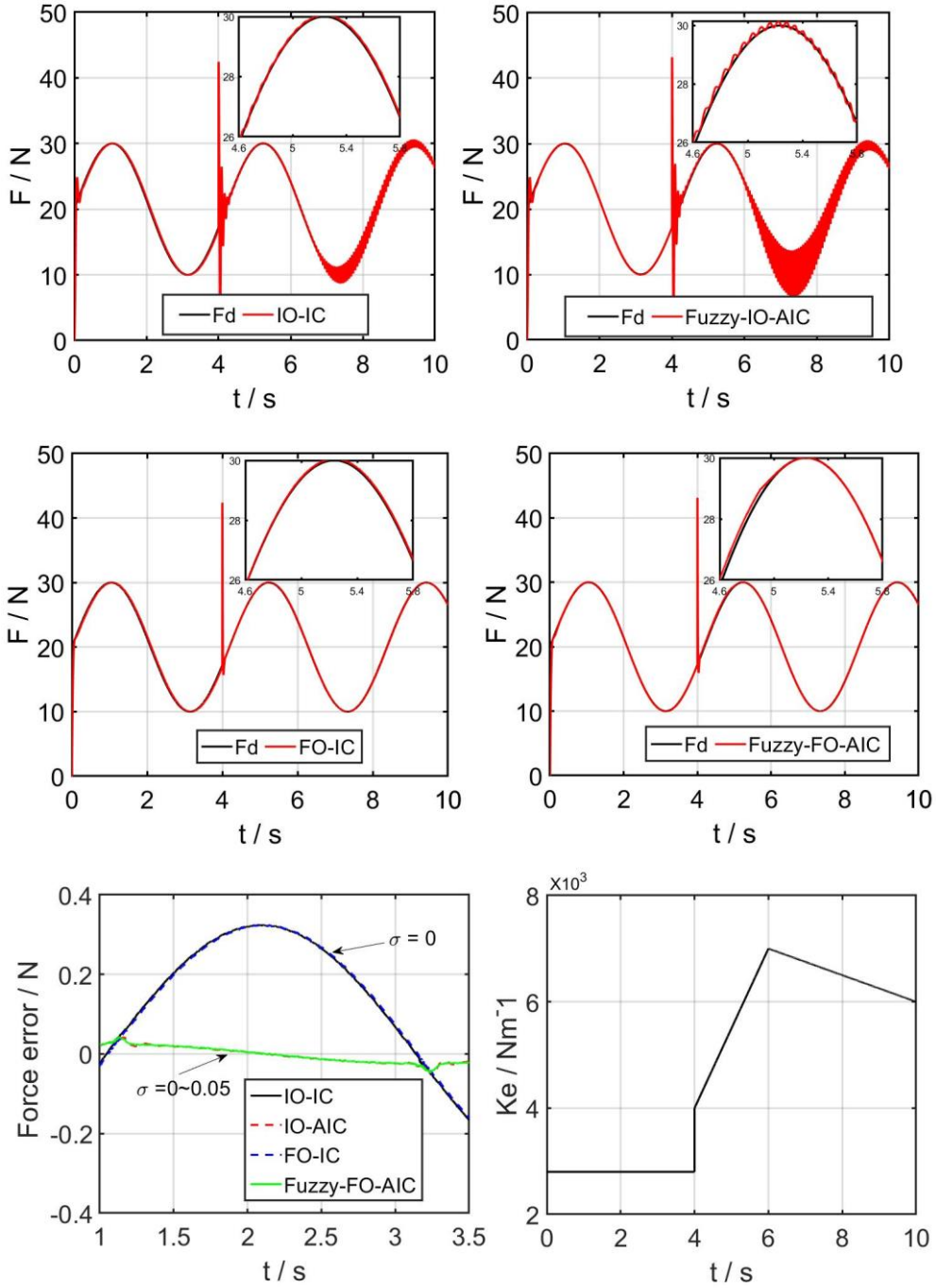

Figure 9 Comparison of force tracking performance between IO and FO impedance in a high-stiffness environment.

4.2 Quadruped robot walking process simulation

Figure 10 depicts the dynamic interaction between a quadruped robot and the walking surface environment throughout its locomotion, emphasizing the superior efficacy of pure proportional-derivative (PD) motion control relative to fractional-order impedance control. The parameters associated with the PD control are $k_p = 1e^3$, $k_d = 1e^2$. The main dynamic parameters of the quadruped robot $m_{body} = 2\ \text{kg}, m_{uleg} = 0.5\ \text{kg}, m_{lleg} = 0.5\ \text{kg}$. Fractional order impedance parameters $m_d = 1\ \text{Ns}^2/\text{m}$, $b_d = 50\ \text{Ns/m}$ and $k_d = 1000\ \text{Ns/m}$, the order β is selected as 1.7, and the sampling period remains consistent with the aforementioned details.

As illustrated in Figure 11, the simulation outcomes indicate that when a quadruped robot descends from a specified height, neither of the control strategies employed effectively reduces the oscillatory overshooting contact force that arises between the robot and the ground. Therefore, it is often necessary to incorporate both active and passive compliance control mechanisms to improve performance in real-world applications. However, once the robot establishes stability on the ground, the use of PD control during locomotion results in significant contact overshoot at the robot's four legs upon engaging with the environment, with peak overshoot forces reaching approximately 70 N. In contrast, the implementation of fractional-order impedance control markedly diminishes the peaks of contact force overshoot, ensuring that all peak forces remain below 50 N. This approach promotes smoother joint output throughout the walking cycle, thereby effectively protecting the joints from recurrent overloads and impacts.

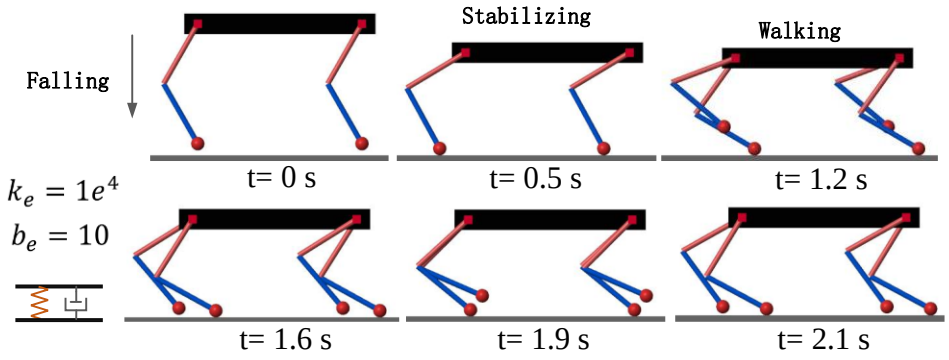

Figure 10 Quadruped robot walking process

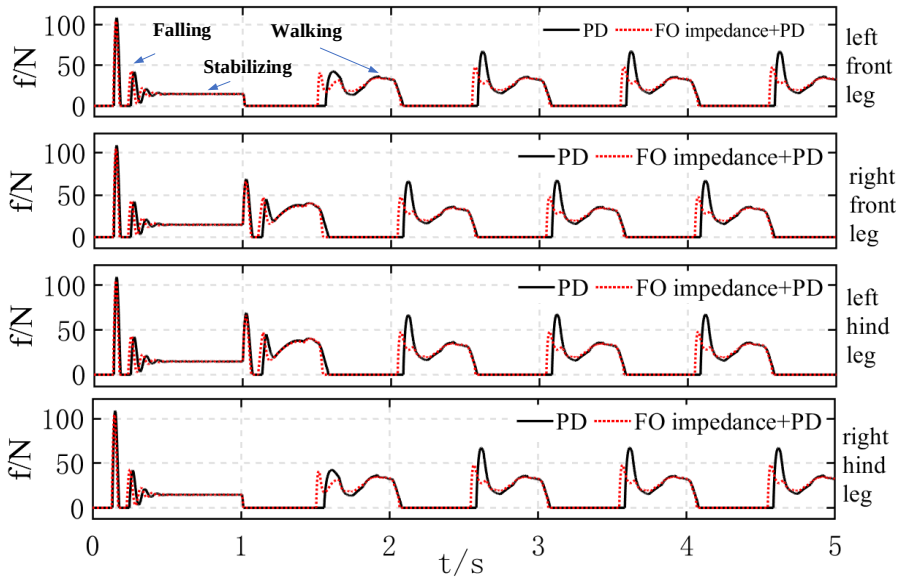

Figure 11 Contact force between the foot end and the ground during walking of a quadruped robot

5. Conclusion

This research paper examines the challenges associated with regulating robot contact dynamics in dynamic and uncertain environments. It proposes the implementation of fractional-order impedance as a means to enhance stability during contact processes. The paper introduces a percentage coefficient transformation grounded in the fundamental properties of fractional-order impedance, in conjunction with adaptive modifications to boundary conditions, to address the computational complexities involved. The study demonstrates that the application of fractional-order

impedance significantly reduces peak contact force overshoot and minimizes unstable oscillations during contact interactions. Overall, the findings indicate that this control strategy is particularly advantageous for managing robotic interactions in unpredictable environments.

This article is the research result of the 2021 Shanxi province basic research plan project (number "202103021223109").

References

[1] Siciliano B, Villani L. Robot force control[M]. Springer Science & Business Media, 2012.

[2] Sun T, Liu H. Adaptive force and velocity control based on intrinsic contact sensing during surface exploration of dynamic objects [J]. Autonomous Robots, 2020, 1-18.

[3] Raibert M H, Craig J J. Hybrid position/force control of manipulators[J]. ASME, J. of Dynamic Systems, Measurement, and Control. 1981, 103(2):126-133.

[4] Mason M T. Compliance and force control for computer-controlled manipulators [J]. IEEE Transactions on Systems, Man, and Cybernetics, 1981, 11(6):418-432.

[5] Hogan N. Impedance control: An approach to manipulation: Part I-Theory. ASME, J. of Dynamic Systems, Measurement, and Control, 1985,107(1):1-7.

[6] Komati B, Pac M R, Ranatunga I, et al. Explicit force control vs impedance control for micromanipulation [C]. Proc. ASME international design engineering technical conferences and computers and information in engineering conference, 2013.

[7] Akdoğan E, Aktan M E, Koru A T, et al. Hybrid impedance control of a robot manipulator for wrist and forearm rehabilitation: Performance analysis and clinical results [J]. Mechatronics, 2018, 49: 77-91.

[8] Jung S, Hsia T C, Bonitz R G. Force tracking impedance control of robot manipulators under unknown environment [J]. IEEE Transactions on Control Systems Technology, 2004, 12(3):474-483.

[9] Duan J, Gan Y, Chen M, et al. Adaptive variable impedance control for dynamic contact force tracking in uncertain environment. Robotics and Autonomous Systems, 2018, 102, 54-65.

[10] Xu, W. Robotic time-varying force tracking in position-based impedance control. ASME, J. of Dynamic Systems, Measurement, and Control. 2016, 138(9): 091008.

[11] Cao H, Chen X, He Y, et al. Dynamic adaptive hybrid impedance control for dynamic contact force tracking in uncertain environments [J]. IEEE Access, 2019, 7: 83162-83174.

[12] Sheng X, Zhang X. Fuzzy adaptive hybrid impedance control for mirror milling system [J]. Mechatronics, 2018, 53:20-27.

[13] Islam M R, Rahmani M, Rahman M H. A Novel Exoskeleton with Fractional Sliding Mode Control for Upper Limb Rehabilitation [J]. Robotica, 2020, 1-22.

[14] Nikdel N, Badamchizadeh M, Azimirad V, et al. Fractional-order adaptive backstepping control of robotic manipulators in the presence of model uncertainties and external disturbances [J]. IEEE Transactions on Industrial Electronics,2016, 63(10):6249-6256.

[15] Aydin Y, Tokatli O, Patoglu V, et al. Stable physical human-robot interaction using fractional order admittance control [J]. IEEE transactions on haptics, 2018,11(3): 464-475.

[16] Ahmed S, Wang H, Tian Y. Robust Adaptive Fractional Order Terminal Sliding Mode Control for Lower Limb Exoskeleton [J]. Asian Journal of Control, 2019, 21(1):473-482.

[17] Oustaloup A, Levron F, Mathieu B, et al. Frequency-band complex noninteger differentiator: characterization and synthesis [J]. IEEE Trans Circuits System, 2000, 47(1):25‑39.

[18] Dietrich A, Ott C. Hierarchical Impedance-Based Tracking Control of Kinematically Redundant Robots[J]. IEEE Transactions on Robotics, 2020, 36(1):204-221.

[19] Cao H, Y He, Chen X, et al. Smooth adaptive hybrid impedance control for robotic contact force tracking in dynamic environments[J]. Industrial Robot: An International Journal, 2020.

[20] Cavenago F, Voli L, Massari M. Adaptive hybrid system framework for unified impedance and admittance control[J]. Journal of Intelligent & Robotic Systems, 2018, 91(3): 569-581.